

## Thermoelectric Detection of Chiral Heat Transport in Graphene in the Quantum Hall Regime

Seung-Geol Nam,<sup>1</sup> E. H. Hwang,<sup>2</sup> and Hu-Jong Lee<sup>1,\*</sup>

<sup>1</sup>*Department of Physics, Pohang University of Science and Technology, Pohang 790-784, Republic of Korea*

<sup>2</sup>*SKKU Advanced Institute of Nanotechnology, Sungkyunkwan University, Suwon 440-746, Republic of Korea*

(Received 4 March 2013; published 29 May 2013)

We report measurements of heat transport along the edge conducting channels in monolayer graphene in the integer quantum Hall regime. Hot charge carriers are injected to the edge channels, and the thermoelectric voltage is measured at a distance along the edge from the heat injection point. We confirm that heat transport in graphene in the quantum Hall regime is chiral and the thermoelectric signal is correlated with the charge conductance of ballistic transport, following the Mott relation. The thermoelectric signal decays with distance from the heater, indicating that carriers are partially thermalized during edge transmission.

DOI: [10.1103/PhysRevLett.110.226801](https://doi.org/10.1103/PhysRevLett.110.226801)

PACS numbers: 73.43.-f, 72.15.Jf, 72.80.Vp, 73.50.Lw

Graphene, a single-atomic-layer lattice of carbon atoms, has remarkable electronic quantum characteristics, which primarily result from the massless low-energy Dirac-fermionic nature of the charge carriers [1–4]. Recently, much interest has focused on heat and thermoelectric transport in graphene. Thermoelectric transport, related to the energy derivatives of the charge transport coefficient, is more sensitive to changes in the carrier scattering rates than charge transport itself. As such, it provides a useful tool to probe key physical mechanisms affecting the charge carrier dynamics in graphene [5–11]. The extremely weak coupling between low-energy electrons and acoustic phonons in graphene [12,13], in particular, at low temperatures, constitutes a bottleneck in the cooling of hot electrons. As heat transport is primarily via charge carriers, it can be used to get an insight into the energy-relaxation mechanisms of carriers in graphene [14–17].

In this Letter, we report heat transport in graphene in the quantum Hall (QH) regime. The unique QH electrical transport properties of graphene are among the most remarkable consequences of the Dirac-fermionic excitations in the material, which lead to the quantized QH plateaus in odd multiples of  $2e^2/h$  [18,19]. In the QH state, charge carriers are confined to the edge conducting channels and circulate either clockwise or counterclockwise depending on the direction of the magnetic field and the type of the charge carriers. We show that the QH heat transport is also confined along the edge conducting channels, and our measurements show, for the first time, that the Mott relation [20] holds between the QH heat transport and the ballistic charge transport along the edge channels [21]. Our study also provides a separate tool, other than electrical, to probe details of the edge-state equilibration at the interface between regions of different filling factors in graphene. The thermoelectric signal is observed to decay with distance from the heater, a sign that part of the heat is transferred out of the edge channels. This can be used to obtain valuable information about the coupling between

charge carriers in the edge channels and various carrier-thermalization factors (such as acoustic phonons in graphene), which has been studied recently in semiconducting two-dimensional electron gas systems [22,23].

To observe the heat transport along the QH edge channels in graphene, we essentially adopt the scheme in Ref. [24] for generating hot carriers and detecting the corresponding thermoelectric signal. Figure 1(a) shows a schematic diagram of the device and measurement configuration, with Ohmic contacts attached along three of the edges of a large rectangular graphene sheet. Figure 1(b) shows the corresponding optical image of the device. Monolayer graphene, with the carrier mobility of  $\sim 5000$  cm<sup>2</sup>/(V s), is prepared by mechanical exfoliation on a highly doped *n*-type Si substrate capped with a 300-nm-thick SiO<sub>2</sub> layer. The contacts are defined by using electron-beam lithography, and a 5/35-nm-thick Ti/Au stack is deposited and selectively removed by using lift-off. Then, the graphene layer is etched into a  $20\ \mu\text{m} \times 3\ \mu\text{m}$  rectangle with three narrow constrictions on the top edge by using an oxygen plasma. The solid line in Fig. 1(b) shows the boundary of the graphene layer. Each constriction is 500 nm wide and  $3\ \mu\text{m}$  long, and the center-to-center distance between adjacent constrictions is  $\sim 8\ \mu\text{m}$ . Finally, an air-bridge-type suspended local gate is fabricated above each constriction by using a multilevel lithography technique [25]. These local gates, together with the global back gate (i.e., doped silicon substrate), are used to control the carrier density and the conductance of both the bulk of graphene and each graphene constriction. The suspended gates are used so that the temperature distribution over the constriction regions of graphene would not be disturbed during the thermoelectric measurements. Hot carriers are injected at one location at the edge of the graphene sheet, and transport is observed by measuring the thermoelectric signal using a detector placed at a distance from the injector. The thermoelectric signal arises from the temperature difference across a detector constriction. Measurements are made by using a

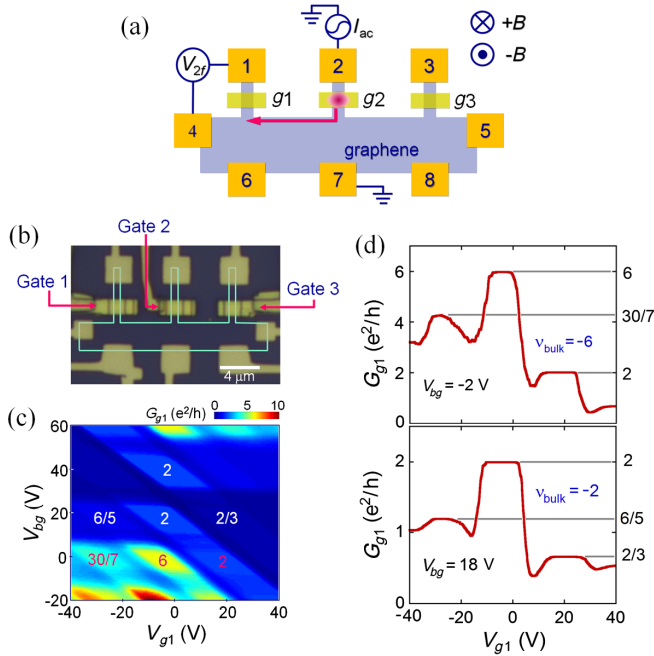


FIG. 1 (color online). (a) Schematic diagram showing the configuration of the devices used. An excitation current modulated at a frequency  $f$  is injected through the center constriction, while the thermoelectric  $2f$  components of the voltage difference are detected between contacts 1 and 4 (or between contacts 3 and 5). The contacts are shown by the numbered rectangles. (b) Optical image of a typical device. The solid line shows the boundary of the graphene layer with three constrictions. A suspended gate is placed above each constriction. (c) Two-terminal conductance between contacts 1 and 6 ( $G_{g1}$ ) as a function of the back gate voltage ( $V_{bg}$ ) and the voltage on gate 1 ( $V_{g1}$ ), measured at  $B = -16$  T and at a lattice temperature of  $T_{ph} = 100$  mK. (d) Dependence of the conductance on  $V_{g1}$  at  $V_{bg} = -2$  V (upper) and  $V_{bg} = -18$  V (lower). The gray horizontal lines show the expected two-terminal QH conductance plateaus with the conductance values denoted in units of  $e^2/h$ .

conventional lock-in technique (at a frequency of 7 Hz) with devices mounted in a dilution fridge at the lattice temperature of  $T_{ph} = 100$  mK and in magnetic fields up to 16 T.

Joule heating is realized by applying a current between contacts 2 and 7, through the center constriction, while tuning the conductance off a QH plateau (i.e., in a transition region) by varying the voltage on local gate 2 ( $V_{g2}$ ). At sufficiently low  $T_{ph}$ , where the electron-phonon coupling is weak in graphene, most of the heat is transported by charge carriers along the QH edge channels. From the Wiedemann-Franz law, the temperature of the carriers,  $T_{el}$ , in the edge states is enhanced according to  $T_{el}^2 - T_{ph}^2 = 3hP/(|\nu_{bulk}|\pi^2k_B^2)$  [26], where  $h$  is Planck's constant,  $\nu_{bulk}$  is the filling factor of the edge states of the bulk of graphene, and  $k_B$  is Boltzmann's constant. For an edge current circulating counterclockwise,  $T_{el}$  near gate 1 (located downstream) becomes higher than  $T_{ph}$ , with the temperature difference  $\Delta T = T_{el} - T_{ph}$  across the graphene

constriction below local gate 1. If the filling factor of the left constriction deviates from  $\nu_{bulk}$  by tuning the voltage on local gate 1 ( $V_{g1}$ ), a thermoelectric voltage  $\Delta V$  is induced between contacts 1 and 4.  $\Delta V$  is given by  $\Delta V = \int_{T_{ph}}^{T_{el}} S_{g1} dT$ , where  $S_{g1}$  is the thermoelectric power of the graphene constriction below gate 1 (see Supplemental Material [27]).

In our devices, where we can independently control the back gate voltage  $V_{bg}$  and the local gate voltages, the QH conductance distribution along a constriction becomes more complicated than the occurrence of simple conductance plateaus at odd multiples of  $2e^2/h$  in bulk graphene. The edge states develop independently with separate filling factors of  $\nu_i$  ( $i = g1, g2, g3$ ) for the local-gated regions and with  $\nu_{bulk}$  for the bulk of graphene. Equilibration of the edge states at the boundary of local-gated regions leads to a quantized two-terminal conductance at a fraction of  $e^2/h$ , depending on the relative magnitude and sign of  $\nu_i$  and  $\nu_{bulk}$  [28–30] (see Supplemental Material [27]).

Figure 1(c) shows the measured two-terminal conductance between contacts 1 and 6 ( $G_{g1}$ ) as a function of  $V_{bg}$  and  $V_{g1}$  for  $B = -16$  T [see Fig. 1(a) for the convention of the field direction]. The conductance map consists of adjoining parallelograms of different conductance, which correspond to different combinations of  $\nu_{bulk}$  and  $\nu_{g1}$ . Similar conductance maps are obtained for the other two constrictions (see Supplemental Material [27]). To provide a quantitative comparison, in Fig. 1(d) we plot  $G_{g1}$  as a function of  $V_{g1}$  for  $\nu_{bulk} = -6$  (upper panel) and  $\nu_{bulk} = -2$  (lower panel). Plateaus for the expected conductance in units of  $e^2/h$  (see Supplemental Material [27]) are shown by the gray horizontal lines. In both graphs, the measured plateaus are in excellent agreement with the expected values. In particular, for  $\nu_{bulk} = -2$  and  $\nu_{g1} = -2$  (corresponding to  $V_{g1} = -10$ – $-1$  V), a quantized conductance plateau at  $2e^2/h$  is clearly seen, which is usually absent for disordered local-gated boundaries of graphene [28]. This demonstrates that we have formed high-quality gate boundaries in our device by using the suspended gates.

For  $B = -16$  T, holelike carriers in the edge states circulate counterclockwise. Thus, for hot-hole injection from the center constriction, it is expected that the thermoelectric voltage will appear at the left detector. To examine this chiral character, we apply a low-frequency modulated current ( $I = 1$ – $40$  nA at  $f \sim 7$  Hz) from contact 2 to 7 and measure the thermoelectric voltage difference between contacts 1 and 4. Because Joule heating is proportional to  $I^2$ , the signal at a frequency  $2f$  that is  $-90^\circ$  out of phase with the heating current corresponds only to the thermoelectric voltage  $V_{2f}$  ( $\equiv \Delta V$ , introduced above), which is separate from the regular electrical conductance signal (i.e., the  $1f$  signal). The thermoelectric power is known to vanish at QH plateaus [5–7, 11, 31, 32]. Thus, to measure

$V_{2f}$ ,  $G_{g1}$  is adjusted to a transition region between two adjacent QH plateaus, setting  $S_{g1}$  to be nonvanishing.

We observe the dependence of  $V_{2f}$  on the heater resistance by varying the two-terminal  $1f$  resistance between contacts 2 and 7 ( $R_{g2}$ ). Figure 2(a) shows measured  $V_{2f}$  and  $R_{g2}$  in  $B = -16$  T as a function of  $V_{g2}$  for  $\nu_{\text{bulk}} = -6$  with various excitation currents, and Fig. 2(b) shows this for  $\nu_{\text{bulk}} = -2$ .  $V_{2f}$  and  $R_{g2}$  show a very similar dependence on  $V_{g2}$ , implying a close relationship between the two quantities. Note that  $R_{g2}$  is the total two-terminal resistance, which is a series combination of the interfacial resistance  $h/(|\nu_{\text{bulk}}|e^2)$ , arising at the boundary of heater contacts 2 and 7, and the resistance across the local-gated region of the center constriction. However, Joule heating generated at the contact immediately sinks to the heat reservoir (i.e., the contact pads 2 and 7) so that actual heating is generated only over the local-gated region with the relevant heater resistance of  $R_{g2} - h/(|\nu_{\text{bulk}}|e^2)$ . For this reason,  $V_{2f}$  vanishes as  $R_{g2} \rightarrow h/(|\nu_{\text{bulk}}|e^2)$ , as shown in Figs. 2(a) and 2(b), where no backscattering (thus, no heating) takes place at the heater constriction.

Figure 2(c) shows the dependence of  $V_{2f}$  on the heating power,  $P = I^2[R_{g2} - h/(|\nu_{\text{bulk}}|e^2)]$ , measured by varying  $R_{g2}$  for various excitation currents  $I$ . For both  $\nu_{\text{bulk}} = -2$  and  $\nu_{\text{bulk}} = -6$ , all data points tend to fall onto respective single curves, indicating that the observed  $V_{2f}$  arises from Joule heating at the center constriction. Provided all the

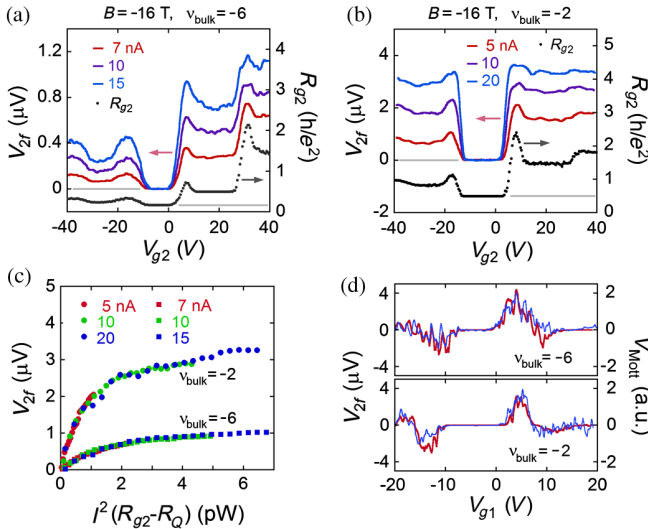


FIG. 2 (color online). (a),(b) Thermoelectric voltage between contacts 1 and 4 ( $V_{2f}$ ) and two-terminal resistance between contacts 2 and 7 ( $R_{g2}$ ) as a function of the voltage of gate 2 ( $V_{g2}$ ). Measurements are made at (a)  $V_{bg} = -2$  V,  $V_{g1} = 6.3$  V, and (b)  $V_{bg} = 18$  V,  $V_{g1} = 4.8$  V. (c)  $V_{2f}$  as a function of heating power.  $V_{2f}$  is measured by varying  $R_{g2}$  for different excitation currents for  $\nu_{\text{bulk}} = -6$  and  $-2$ . (d) Dependence of  $V_{2f}$  on  $V_{g1}$  at  $V_{bg} = -2$  V (upper) and  $V_{bg} = 18$  V (lower) for  $I = 40$  nA. Calculations of  $V_{2f}$  from the Mott relation are shown for comparison.

Joule heating is transported by the edge current, and that the Mott relation is valid (i.e.,  $S_{g1} = \beta T$ , for a coefficient  $\beta$ ),  $V_{2f}$  is expected to be proportional to the heating power, as  $V_{2f} = \int_{T_{\text{ph}}}^{T_{\text{el}}} S_{g1} dT = (\beta/2)(T_{\text{el}}^2 - T_{\text{ph}}^2) \propto P$ . From Fig. 2(c), however, we can see that  $V_{2f}$  varies linearly with  $P$  only for low  $P$ , and, when  $P > 1$  pW,  $V_{2f}$  increases sublinearly and saturates at high  $P$ . This is attributed to power dissipation via acoustic phonons in graphene at the heater constriction (see Supplemental Material [27]).

Now, we examine the effect of modulating the conductance of the detector constriction on  $V_{2f}$ . Figure 2(d) shows  $V_{2f}$  as a function of  $V_{g1}$  for  $\nu_{\text{bulk}} = -6$  and  $\nu_{\text{bulk}} = -2$ , with  $G_{g2}$  adjusted to a transition region between two adjacent QH plateaus. Fluctuations in  $V_{2f}$  are observed with varying  $G_{g1}$  when in transition regions, but it vanishes when  $G_{g1}$  exhibits plateaus [refer to Fig. 1(d)]. The Mott relation [20] states that the thermoelectric power is proportional to the energy derivatives of the logarithm of the conductance,  $S_{g1} \sim -d \ln G_{g1} / dE|_{E_F}$ . In Fig. 2(d), we show  $V_{\text{Mott}} = -\alpha d \ln G_{g1} / dV_{g1} \propto S_{g1}$  calculated for a fixed  $\Delta T$ , where  $\alpha = \sqrt{|en_1/C_{g1}|}$ ,  $C_{g1}$  is the capacitance of local gate 1, and  $n_1$  is the average carrier density of the left constriction (see Supplemental Material [27]). As shown in Fig. 2(d), the measured  $V_{2f}$  is in good agreement with the Mott prediction [33]. The validity of the Mott relation is further evidence that the observed  $2f$  signal is thermoelectric in origin, arising from the temperature difference between the hot electrons constituting the edge current and the thermal reservoir (i.e., the lattice) across the detector constriction. Even the fluctuations in  $V_{2f}$ , which originate from the coherent universal conductance fluctuations in  $G_{g1}$ , tend to be reproduced in  $V_{\text{Mott}}$ . In the bipolar regime with  $p$ - $n$  interfaces [i.e., the region of  $V_{g1} > 8$  V for  $\nu_{\text{bulk}} = -2$  of the lower panel of Fig. 2(d)],  $V_{2f}$  shows larger fluctuations than the Mott prediction, which may arise from enhanced scattering at the  $p$ - $n$  interfaces. The overall heater- and detector-voltage dependence of  $V_{2f}$  for  $\nu_{\text{bulk}} = -2$  is summarized in the Supplemental Material [27].

For a detector located upstream of the heater, the  $V_{2f}$  signals are expected to vanish as the hot carriers are thermalized at the cold contacts during the chiral flow along the entire conducting path from heater to detector. With the inversion of the chirality when the direction of the magnetic field is reversed (i.e.,  $+16$  instead of  $-16$  T),  $V_{2f}$  vanishes at the left constriction (i.e., at gate 1), and it appears at the right one (at gate 3), as shown in Fig. 3(a). In our graphene layer, with the gapless band structure and the low carrier density, chirality of the edge charge transport is easily controlled by tuning the carrier type of the bulk of graphene with back gating. Thus, as the chirality changes again by reversing the carrier type from holes to electrons,  $V_{2f}$  is restored at the left constriction while it vanishes at the right one, as shown in Fig. 3(b). This chiral dependence of  $V_{2f}$  on

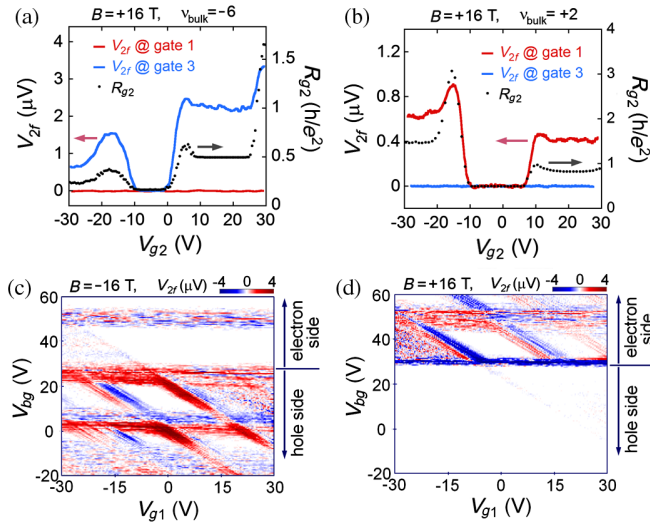


FIG. 3 (color online). (a),(b)  $V_{2f}$  and  $R_{g2}$  at  $B = +16$  T for (a)  $V_{bg} = -5$  V and (b)  $V_{bg} = 36$  V for  $I = 40$  nA.  $V_{2f}$  is measured at both the left- and the right-hand side constrictions. (c),(d)  $V_{2f}$  detected at the left constriction as a function of  $V_{bg}$  and  $V_{g1}$  for (c)  $B = -16$  T and (d)  $B = +16$  T.

the magnetic field direction and the carrier type is more clearly shown in Figs. 3(c) and 3(d), where  $V_{2f}$  is detected at the left constriction as a function of  $V_{bg}$  and  $V_{g1}$  for  $B = -16$  and  $+16$  T, respectively. Here, we apply a sufficiently high gate voltage at gate 2 to satisfy the condition  $G_{g2} \neq e^2/(\nu_{\text{bulk}}|h)$  for all back gate voltages. As expected, in the negative (positive) field direction,  $V_{2f}$  with fluctuations is observed only for holes (electrons), while no clear signals are present for electrons (holes) [34]. There is considerable similarity between the conductance map in Fig. 1(c) and the  $V_{2f}$  map in Figs. 3(c) and 3(d), which again indicates a direct correlation between the electrical conductance and the thermoelectric power. Here, the  $V_{2f}$  signal is more prominent at the boundaries of the conductance parallelograms, which correspond to the QH-conductance transition regions, confirming the condition for observing nonvanishing  $V_{2f}$  signals as discussed above. In comparison with the conductance map shown in Fig. 1(c),  $V_{2f}$  provides more details of the edge equilibrium states in the detector constriction, with the direct confirmation of the flow chirality of the carriers along the edge channels. The observed  $V_{2f}$  maps showing the gradual establishment of chiral heat transport through the edge channels with increasing magnetic field strength are shown in the Supplemental Material [27].

Now, we estimate the range over which hot edge-state carriers propagate before appreciable cooling occurs. Figures 4(a) and 4(b) show  $V_{2f}$  measured between contacts 1 and 4 obtained by using the right-hand constriction as the heater by applying a current from contact 3 to 8. With  $G_{g2}$  adjusted to  $|\nu_{\text{bulk}}|e^2/h$ , all hot carriers from the heater are transmitted through the center constriction without back-scattering and are completely thermalized to the thermal

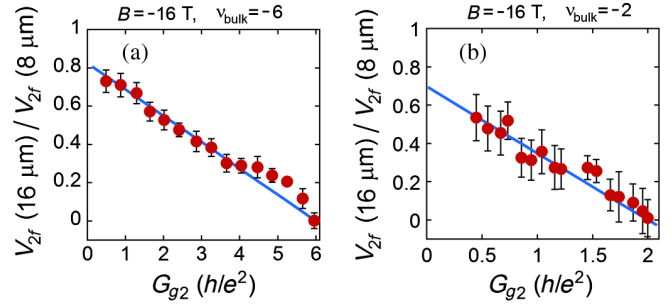


FIG. 4 (color online). (a),(b)  $V_{2f}$  measured at constriction 1 for a  $16\text{-}\mu\text{m}$  heater-detector separation with constriction 3 as the heater, shown as a function of  $G_{g2}$  at (a)  $V_{bg} = -5$  V and (b)  $V_{bg} = 13$  V, for  $B = -16$  T and  $I = 20$  nA. Data are normalized to  $V_{2f}$  for an  $8\text{-}\mu\text{m}$  separation between the heater (constriction 2) and the detector (constriction 1).

reservoir at contact 2. In this case, no heat propagates to the detector with vanishing  $V_{2f}$ , as is the case for  $G_{g2} = 6e^2/h$  and  $2e^2/h$  in Figs. 4(a) and 4(b), respectively. When  $G_{g2} < |\nu_{\text{bulk}}|e^2/h$ , however, only a fraction of the hot carriers from the heater are transmitted to contact 2 to be thermalized. In this case, with a portion of the hot carriers reaching the detector,  $V_{2f}$  has a finite value. Further pinching off the center constriction by reducing  $G_{g2}$  causes more hot carriers to reach the detector constriction, shown by the increase of  $V_{2f}$  as seen in Figs. 4(a) and 4(b). See the Supplemental Material [27] for further analysis of  $V_{2f}$  induced by using the right-hand constriction as a heater.

Since the conductance of graphene remains finite even at the charge-neutrality point [1],  $G_{g2}$  is reduced only to  $\sim 0.4e^2/h$  in our devices. However, one can estimate the hypothetical value of  $V_{2f}$  for completely vanishing  $G_{g2}$  by linearly extrapolating the  $V_{2f}$  data as shown in Figs. 4(a) and 4(b) to the limit of  $G_{g2} = 0$ . This procedure is justified, because  $V_{2f}$  is proportional to the Joule heating power  $P$  entering the detector, which increases as the center constriction is pinched off in proportion to  $|\nu_{\text{bulk}}|e^2/h - G_{g2}$ . Here, the data are normalized to  $V_{2f}$  measured at the same detector but employing the center constriction as the heater. In Figs. 4(a) and 4(b), the normalized  $V_{2f}$  at  $G_{g2} = 0$  turns out to be less than unity, which indicates that hot carriers are partially cooled as they propagate along the edge channels. A similar result was obtained in GaAs/AlGaAs two-dimensional electron gases when  $\nu_{\text{bulk}} = 1$  [24]. Assuming that the  $2f$  signal decays exponentially with distance ( $L$ ) between the heater and detector as  $V_{2f}(L) = V_{2f}(0) \times \exp(-L/\ell_{\text{in}})$ , the thermal decay length in our device is estimated to be  $\ell_{\text{in}} \sim 22\text{ }\mu\text{m}$  for  $\nu_{\text{bulk}} = -2$  and  $\sim 36\text{ }\mu\text{m}$  for  $\nu_{\text{bulk}} = -6$ .

Carrier cooling may be expected to be dominated by the emission of acoustic phonons at the right-hand heater constriction in the QH transition region. However, by referring to the normalized  $V_{2f}$  signal in Fig. 4, the possibility of the carrier cooling via phonon excitations at a heater

constriction is excluded, assuming similar electron-phonon coupling strength in the QH-conductance transition region at the two heater constrictions. It is also possible that the carriers are cooled via coupling with acoustic phonons during the edge propagation. However, since the electron-phonon coupling along an edge channel is expected to be suppressed exponentially with temperature as  $\exp(-T^*/T)$ , where  $T^* \sim 15$  K [35], the electron-phonon coupling at our measurement temperature should be too small to account for the carrier cooling during the edge propagation.

Disorder can induce localized states in the bulk, which can couple with the edge states via Coulomb interactions. This energy transfer mechanism may allow a part of the heat generated at the top of the graphene sheet to be carried away to the bottom, providing a possible cooling path for hot carriers. Low-energy bulk excitation is also expected in the spin sector in graphene for certain filling factors [36]. However, these spin excitations may not be present in our measurements where all Landau-level multiplets are either completely filled or empty. Further studies are required to clarify the exact cause of the heat loss along the edge channels in graphene.

In conclusion, we have measured heat transport in the integer QH regime in devices prepared on monolayer graphene. Our measurements clearly indicate that heat transport in the QH regime is confined in the edge conducting channels, with flow chirality depending on the magnetic field direction and the carrier type. This provides a convenient means of guiding heat in a mesoscopic-scale graphene sheet. The spatial confinement of heat transport and the directivity of the flow allow accurate estimation of the partial heat loss during the propagation through graphene. Our thermal transport measurements offer a new tool to probe low-energy excitations in graphene-based QH systems, which cannot be investigated by using electrical conductance measurements.

This work was supported by the National Research Foundation through the SRC Center for Topological Matter (Grant No. 2011-0030788) and the GFR Center for Advanced Soft Electronics (Grant No. 2011-0031640).

\*Corresponding author.

hjlee@postech.ac.kr

- [1] A. K. Geim and K. S. Novoselov, *Nat. Mater.* **6**, 183 (2007).
- [2] M. I. Katsnelson, K. S. Novoselov, and A. K. Geim, *Nat. Phys.* **2**, 620 (2006).
- [3] C. H. Park, Y.-W. Son, L. Yang, M. L. Cohen, and S. G. Louie, *Nano Lett.* **8**, 2920 (2008).
- [4] V. V. Cheianov, V. Fal'ko, and B. L. Altshuler, *Science* **315**, 1252 (2007).
- [5] Y. M. Zuev, W. Chang, and P. Kim, *Phys. Rev. Lett.* **102**, 096807 (2009).
- [6] P. Wei, W. Bao, Y. Pu, C. N. Lau, and J. Shi, *Phys. Rev. Lett.* **102**, 166808 (2009).
- [7] J. G. Checkelsky and N. P. Ong, *Phys. Rev. B* **80**, 081413 (R) (2009).

- [8] E. H. Hwang, E. Rossi, and S. Das Sarma, *Phys. Rev. B* **80**, 235415 (2009).
- [9] D. Wang and J. Shi, *Phys. Rev. B* **83**, 113403 (2011).
- [10] C. R. Wang, W.-S. Lu, L. Hao, W.-L. Lee, T.-K. Lee, F. Lin, I.-C. Cheng, and J.-Z. Chen, *Phys. Rev. Lett.* **107**, 186602 (2011).
- [11] S.-G. Nam, D.-K. Ki, and H.-J. Lee, *Phys. Rev. B* **82**, 245416 (2010).
- [12] K. I. Bolotin, K. J. Sikes, J. Hone, H. L. Stormer, and P. Kim, *Phys. Rev. Lett.* **101**, 096802 (2008).
- [13] E. H. Hwang and S. Das Sarma, *Phys. Rev. B* **77**, 115449 (2008).
- [14] S. S. Kubakaddi, *Phys. Rev. B* **79**, 075417 (2009).
- [15] J. K. Viljas and T. T. Heikkila, *Phys. Rev. B* **81**, 245404 (2010).
- [16] A. C. Betz *et al.*, *Phys. Rev. Lett.* **109**, 056805 (2012).
- [17] A. C. Betz, S. H. Jhang, E. Pallecchi, R. Ferreira, G. Fève, J.-M. Berroir, and B. Plaçais, *Nat. Phys.* **9**, 109 (2013).
- [18] K. S. Novoselov, A. K. Geim, S. V. Morozov, D. Jiang, M. I. Katsnelson, I. V. Grigorieva, S. V. Dubonos, and A. A. Firsov, *Nature (London)* **438**, 197 (2005).
- [19] Y. Zhang, Y. W. Tan, H. L. Stormer, and P. Kim, *Nature (London)* **438**, 201 (2005).
- [20] M. Cutler and N. F. Mott, *Phys. Rev.* **181**, 1336 (1969).
- [21] U. Sivan and Y. Imry, *Phys. Rev. B* **33**, 551 (1986).
- [22] H. le Sueur, C. Altimiras, U. Gennser, A. Cavanna, D. Maily, and F. Pierre, *Phys. Rev. Lett.* **105**, 056803 (2010).
- [23] C. Altimiras, H. le Sueur, U. Gennser, A. Cavanna, D. Maily, and F. Pierre, *Phys. Rev. Lett.* **105**, 226804 (2010).
- [24] G. Granger, J. P. Eisenstein, and J. L. Reno, *Phys. Rev. Lett.* **102**, 086803 (2009).
- [25] G. Liu, J. Velasco, W. Bao, and C. N. Lau, *Appl. Phys. Lett.* **92**, 203103 (2008).
- [26] C. L. Kane and M. P. A. Fisher, *Phys. Rev. B* **55**, 15 832 (1997).
- [27] See Supplemental Material at <http://link.aps.org/supplemental/10.1103/PhysRevLett.110.226801> for supplemental data and detailed data analysis.
- [28] B. Ozyilmaz, P. Jarillo-Herrero, D. Efetov, D. Abanin, L. Levitov, and P. Kim, *Phys. Rev. Lett.* **99**, 166804 (2007).
- [29] S.-G. Nam, D.-K. Ki, J. W. Park, Y. Kim, J. S. Kim, and H.-J. Lee, *Nanotechnology* **22**, 415203 (2011).
- [30] D.-K. Ki, S.-G. Nam, H.-J. Lee, and B. Ozyilmaz, *Phys. Rev. B* **81**, 033301 (2010).
- [31] S. M. Girvin and M. Johnson, *J. Phys. C* **15**, L1147 (1982).
- [32] M. Jonson and S. M. Girvin, *Phys. Rev. B* **29**, 1939 (1984).
- [33] The Mott relation is valid, in general, for diffusive transport of carriers in equilibrium with lattice. However, its validity has been shown theoretically to be extended to ballistic transport [21], such as the QH-edge conduction.
- [34] The horizontal band of the nonvanishing  $V_{2f}$  signal seen in the electron side of Fig. 3(c) corresponds to a QH-conductance transition region with the highest-index Landau-level edge channel disappearing in the bulk of graphene. A consequence is that, as the heat flow partially loses the chiral characteristics, a nonvanishing  $V_{2f}$  signal arises, irrespective of the carrier type. However, it is not understood why a similar nonvanishing  $V_{2f}$  signal is not present in the hole side of Fig. 3(d).
- [35] T. Martin and S. Feng, *Phys. Rev. Lett.* **64**, 1971 (1990).
- [36] K. Yang, S. Das Sarma, and A. H. MacDonald, *Phys. Rev. B* **74**, 075423 (2006).